



**HAL**  
open science

# Novel superhard boron nitrides, B<sub>2</sub>N<sub>3</sub> and B<sub>3</sub>N<sub>3</sub>: Crystal chemistry and first-principles studies

Samir Matar, Vladimir Solozhenko

► **To cite this version:**

Samir Matar, Vladimir Solozhenko. Novel superhard boron nitrides, B<sub>2</sub>N<sub>3</sub> and B<sub>3</sub>N<sub>3</sub>: Crystal chemistry and first-principles studies. *Molecules*, 2024, 29 (17), pp.4052. 10.3390/molecules29174052 . hal-04679721

**HAL Id: hal-04679721**


**<https://hal.science/hal-04679721>**

Submitted on 28 Aug 2024

**HAL** is a multi-disciplinary open access archive for the deposit and dissemination of scientific research documents, whether they are published or not. The documents may come from teaching and research institutions in France or abroad, or from public or private research centers.

L'archive ouverte pluridisciplinaire **HAL**, est destinée au dépôt et à la diffusion de documents scientifiques de niveau recherche, publiés ou non, émanant des établissements d'enseignement et de recherche français ou étrangers, des laboratoires publics ou privés.

# Novel superhard boron nitrides, $B_2N_3$ and $B_3N_3$ : Crystal chemistry and first principles studies

Samir F. Matar  <https://orcid.org/0000-0001-5419-358X>  
Lebanese German University (LGU), Jounieh, P.O. Box 206, Lebanon

Vladimir L. Solozhenko\*  <https://orcid.org/0000-0002-0881-9761>  
LSPM–CNRS, Université Sorbonne Paris Nord, 93430 Villetaneuse, France

## Abstract

Tetragonal and hexagonal hybrid  $sp^3/sp^2$  carbon allotropes  $C_5$ , proposed on the basis of crystal chemistry, were subsequently used as template structures to identify new binary phases of the B-N system, specifically tetragonal and hexagonal boron nitrides,  $B_2N_3$  and  $B_3N_3$ . The ground structures and energy-dependent quantities of new phases were computed within framework of the quantum density functional theory (DFT). All four new boron nitrides were found to be cohesive and mechanically (elastic constants) stable. Vickers hardness ( $H_V$ ) evaluated by various models qualifies all new phases as superhard ( $H_V > 40$  GPa). Dynamically, all new boron nitrides were found to be stable from positive phonon frequencies. The electronic band structures reveal mainly conductive behavior due to the presence of  $\pi$  electrons of  $sp^2$ -like hybrid atoms.

**Keywords:** boron nitride; DFT; crystal structure; elastic constants; hardness; phonons; electronic band structures

---

\* Corresponding author ([vladimir.solozhenko@univ-paris13.fr](mailto:vladimir.solozhenko@univ-paris13.fr))

## Introduction

Carbon allotropes that exhibit mechanical properties similar to those of diamond, in particular, extreme hardness, continue to be a subject of significant interest within the scientific community. Both the predominant cubic diamond and the less common hexagonal form ("lonsdaleite") exhibit ultrahardness due to the three-dimensional arrangement of  $C_4$  tetrahedra with purely  $sp^3$ -hybridization of the carbon atoms. In terms of topology, cubic and hexagonal diamonds are the aristotypes, designated as **dia** and **lon**, respectively [1]. This nomenclature is also applicable to other families of carbon allotropes. The introduction of additional carbon atoms results in alterations to the  $C(sp^3)$  lattice of diamond, giving rise to novel  $C(sp^3)/C(sp^2)$  hybrid allotropes that retain the original physical properties, including electronic ones, which can lead to induced metallicity [2]. In the case of the nearest neighbors of carbon, boron and nitrogen, equiatomic cubic boron nitride (cBN) has been synthesized, which is half as hard as diamond but exhibits much higher thermal and chemical stability [3].

Research efforts to identify new superhard phases of compounds of light elements require the use of structure prediction programs such as USPEX [4] and CALYPSO [5]. However, novel structures can also be identified through the application of crystal engineering rationale as presented here. In all cases, such predictions must be validated by the quantitative study of energies and the derived physical properties using first-principles calculations. Over the years, the well-established quantum mechanics framework of the density functional theory (DFT) [6,7] has proven to be the most efficient.

The present paper further develops the field of boron nitrides by proposing novel cohesive and stable hybrid B–N phases. First, tetragonal and hexagonal  $sp^3/sp^2$  hybrid  $C_5$  allotropes were designed by crystal chemistry engineering and subsequently used as templates for the selective substitution of carbon for boron and nitrogen, leading to the sesquinitride  $B_2N_3$ , which was then transformed into the equiatomic  $B_3N_3$  through the insertion of an additional boron atom into  $B_2N_3$ .

Considering that boron nitride is admittedly equiatomic, our challenging prediction of boron sesquinitride is supported to some extent by the previously reported nitrogen-excess tetragonal  $B_2N_3$  [8], but no structural details were provided for this compound. The boron nitride  $B_{116}N_{124}$  fullerene should also be mentioned as nitrogen-rich B–N phase [9]. Among the boron-rich compounds of the B–N system, it is worth mentioning rhombohedral boron subnitride  $B_{13}N_2$  [10], which is a superhard phase [11].

In the present work we show that all predicted novel B–N phases are cohesive, mechanically and dynamically stable, and characterized by high Vickers hardness and metallic-like behavior.

## Computational methodology

The determination of the ground state structures corresponding to the energy minima and the prediction of their mechanical and dynamical properties were carried out within the widely

accepted framework of DFT. The DFT was initially proposed in two publications: in 1964, Hohenberg and Kohn developed the theoretical framework [6], and in 1965, Kohn and Sham established the Kohn-Sham equations for practical solution of the wave equation [7].

Based on the DFT, calculations were performed within the Vienna Ab initio Simulation Package (VASP) code [12,13] and the Projector Augmented Wave (PAW) method [13,14] for the atomic potentials. DFT exchange correlation (XC) effects were considered using the generalized gradient approximation (GGA) [15]. Preliminary calculations with the native DFT-XC local density approximation (LDA) [16] resulted in underestimated lattice constants at ambient pressure and were therefore abandoned. Relaxation of the atoms to the ground state structures was performed with the conjugate gradient algorithm according to Press *et al.* [17]. The Blöchl tetrahedron method [18] with corrections according to the Methfessel and Paxton scheme [19] was used for geometry optimization and energy calculations, respectively. Brillouin-zone (BZ) integrals were approximated by a special  $\mathbf{k}$ -point sampling according to Monkhorst and Pack [20]. Structural parameters were optimized until atomic forces were below 0.02 eV/Å and all stress components were  $< 0.003$  eV/Å<sup>3</sup>. The calculations were converged at an energy cutoff of 400 eV for the plane-wave basis set in terms of the  $\mathbf{k}$ -point integration in the reciprocal space from  $k_x(6) \times k_y(6) \times k_z(6)$  up to  $k_x(12) \times k_y(12) \times k_z(12)$  to obtain a final convergence and relaxation to zero strains for the original stoichiometries presented in this work, after a systematic upgrade of the structure input file throughout the successive cycles of calculations. In the post-processing of the ground state electronic structures, the charge density projections were operated on the lattice sites.

The investigation of the mechanical properties was based on the calculations of the elastic properties determined by performing finite distortions of the lattice and deriving the elastic constants from the strain-stress relationship. The treatment of the results was done using ELATE online tool devoted to the analysis of the elastic tensors [21]. The program provides the bulk ( $B$ ), shear ( $G$ ) and Young's ( $E$ ) moduli along different averaging methods; the Voigt method [22] was used here. Two empirical models, Mazhnik-Oganov [23] and Chen-Niu [24], were used to estimate the Vickers hardness ( $H_V$ ) from the elastic constants.

Vickers hardness was also evaluated in the framework of the thermodynamic model [25,26], which is based on thermodynamic properties and crystal structure, and using the Lyakhov-Oganov approach [27], which considers the topology of the crystal structure, the strength of covalent bonds, the degree of ionicity, and directionality. Fracture toughness ( $K_{Ic}$ ) was estimated using the Mazhnik-Oganov model [23].

The dynamic stabilities were confirmed by the positive phonon magnitudes. The corresponding phonon band structures were obtained from a high resolution of the tetragonal and hexagonal Brillouin zones according to Togo *et al.* [28]. The electronic band structures were obtained using the all-electron DFT-based ASW method [29] and the GGA XC functional [15]. The VESTA (Visualization for Electronic and Structural Analysis) program [30] was used to visualize the crystal structures and charge densities.

## Crystal chemistry

### *Tetragonal and hexagonal pentacarbon allotropes*

***tet*-C<sub>5</sub>.** Recently, the body-centered tetragonal carbon allotrope C<sub>4</sub> (*tet*-C<sub>4</sub>) in the space group *I*-4*m*2 (No. 119) [31] (Fig. 1a) has been proposed to serve as a template for the design of the related phases. The four atoms of the unit cell are detailed in Table 1, considering the structure in simple tetragonal arrangement. The subsequent transformation into C<sub>5</sub> consists in keeping the body center carbon (C1 at  $\frac{1}{2}, \frac{1}{2}, \frac{1}{2}$ ), which becomes in C(1c) Wyckoff position (follow the transformation arrows), as well as the two C2, whereby C2a and C2b become C3(2g) and the *z* coordinate becomes  $\pm z'$  instead of  $\pm \frac{1}{4}$ . The additional carbon C2 is provided by parameterizing the *z* position of C1b, resulting in a two-fold C2 (2e) at 0, 0,  $\pm z$ . After full geometry relaxation, the resulting structure retains the tetragonal symmetry now resolved in space group *P*-4*m*2 (No. 115). The structure is shown in Fig. 1b with colored spheres corresponding to the three carbon sites given by the coordinates in Table 1, i.e. with well determined  $z = \pm 0.854$  and  $z' = \pm 0.314$ . Using the TopCryst crystallography package [32], *tet*-C<sub>5</sub> was identified with **3,4<sup>^</sup>2T1-CA** topology. A similar topology was found for another tetragonal carbon allotrope, C<sub>5</sub>, predicted by Wei *et al.* [33] using the CALYPSO code. Note that the initial *tet*-C<sub>4</sub> has a **dia** topology.

***h*-C<sub>5</sub>.** Lonsdaleite (space group *P*6<sub>3</sub>/*m**m**c*, No. 194) is the rare hexagonal form of diamond, *h*-C<sub>4</sub>, which is characterized by a single four-fold atomic position for carbon at  $\frac{1}{3}, \frac{2}{3}, z$  with a small (0.06275) *z*-value along the hexagonal vertical axis. Changing *z* to 0 gives a 2D graphite-like carbon structure (Fig. 2a) with **hcb** topology. Then, the puckering of the graphite-like layers is a key factor in the transition from 2D to 3D structure. Here we model the 2D → 3D transformation by inserting a carbon atom between the carbon layers, as shown by the white sphere in Fig. 2b. Subsequent geometry relaxation yielded a new 3D structure with C<sub>5</sub> stoichiometry (Fig. 2c). The crystal data with three different carbon positions and a symmetry reduction to *P*-6*m*2 (No. 187) are presented in Table 1. The topology is now **lon**, i.e. lonsdaleite-like. The bottom row shows the total energy after full geometry relaxation, which is found to be larger for *tet*-C<sub>5</sub> than for *h*-C<sub>5</sub>. The result can be translated into the average cohesive energy per atom,  $E_{\text{coh}}/\text{atom}$ , which is obtained after subtracting the atomic energy of the carbon atom in a large box, i.e. -6.6 eV. Then the cohesive energy is -2.05 eV for *tet*-C<sub>5</sub> versus -1.90 eV for *h*-C<sub>5</sub>. Both values remain smaller than  $E_{\text{coh}}/\text{atom} = -2.49$  eV for diamond.

### *New tetragonal and hexagonal boron nitrides*

**B<sub>2</sub>N<sub>3</sub>.** C<sub>5</sub> structure was subsequently used as a template to design boron sesquinitride, B<sub>2</sub>N<sub>3</sub>, in both tetragonal and hexagonal forms. Table 2 shows the corresponding atomic substitutions of carbon at the three different positions of Table 1 by boron and nitrogen. The geometry converged atomic positions were found to be close to the matrix C<sub>5</sub> allotropes. It can be observed that the cell volumes of *tet*-B<sub>2</sub>N<sub>3</sub> and *h*-B<sub>2</sub>N<sub>3</sub> are almost the same as well as the total energies with

however a slightly lower value for the former. The crystal structures are shown in Figs. 3 and 4 in ball-and-stick and tetrahedral representations.

**B<sub>3</sub>N<sub>3</sub>**. Subsequently, the equiatomic boron nitride, B<sub>3</sub>N<sub>3</sub>, was designed in both crystal systems by inserting an extra boron at 0, 0, 0 for *tet*-B<sub>3</sub>N<sub>3</sub> and at 1/3, 2/3, 0 for *h*-B<sub>3</sub>N<sub>3</sub> as shown in Table 2 (the 2<sup>nd</sup> and 4<sup>th</sup> data columns). The resulting structures after full geometry relaxation are shown in Figs. 3 and 4. They exhibit a preserved pristine boron sesquinitride structures expanded with additional boron, thus achieving equiatomic stoichiometry. The total energies favor *tet*-B<sub>3</sub>N<sub>3</sub>, which also has a larger volume, indicating a lower density.

Table 2 shows the respective topologies of the new boron nitrides: **3,4<sup>^</sup>2T1-CA** for the tetragonal phases (like pristine C<sub>5</sub>), **lon** for *h*-B<sub>2</sub>N<sub>3</sub> and **tfi** for *h*-B<sub>3</sub>N<sub>3</sub>.

### Projections of the charge densities

To illustrate the electron distribution within the new boron nitrides, the analysis was extended to a qualitative representation of the charge densities. Figs. 3 and 4 (right panels) represent the charge density projections with yellow volumes around the atoms. In all cases, the charges are concentrated around nitrogen atoms (gray spheres). In fact, boron nitride is a polar covalent compound with significant charge transfer to N, which is characterized by an electronegativity of  $\chi_N=3.04$  while  $\chi_B=2.04$  according to the Pauling scale. In B<sub>2</sub>N<sub>3</sub>, the charge gray volumes are squeezed toward the next cell along the vertical *c* direction, corresponding to the N–N connexions between successive cells. By introducing new B–N bonds, equiatomic *tet*-B<sub>3</sub>N<sub>3</sub> and *h*-B<sub>3</sub>N<sub>3</sub> are created, and the charge volumes are around N atoms in both symmetries. Regarding the iso-surface values, the following trends were observed: B<sub>2</sub>N<sub>3</sub>: 0.325; B<sub>3</sub>N<sub>3</sub>: 0.293, i.e. the higher value for the higher nitrogen content.

### Mechanical properties

The analysis of the mechanical properties was carried out by calculating the elastic tensor through finite distortions of the lattice. The calculated sets of elastic constants C<sub>ij</sub> (i and j correspond to directions) of the four new boron nitrides are given in Table 2. All C<sub>ij</sub> values are positive, indicating mechanically stable phases. For comparison, the elastic constants of template *tet*-C<sub>5</sub> and *h*-C<sub>5</sub> are also given. As expected, the carbon allotropes have the largest C<sub>ij</sub> values compared to the compounds of the B–N system. Elastic tensor analysis was performed to obtain the bulk ( $B_v$ ), shear ( $G_v$ ) and Young's ( $E_v$ ) moduli and Poisson's ratio ( $\nu$ ) by Voight's averaging [22] using ELATE software [21]. The calculated elastic moduli, whose values follow the trends observed for C<sub>ij</sub>, are shown in Table 4 along with Vickers hardness values calculated using four contemporary models of hardness [23,24,25,27] and fracture toughness evaluated using the Mazhnik-Oganov model [23].

Since the thermodynamic model is the most reliable in the case of superhard boron compounds [3,37,38] and shows perfect agreement with the available experimental data for cubic boron nitride [40-41], it is obvious that the hardness values calculated within the empirical Mazhnik-Oganov [23] and Chen-Niu [24] models are not reliable. As for the Oganov-Lyakhov model [27], it gives slightly underestimated values, as has already been observed for the superhard compounds of the B–C–N system [38]. It is evident (see Table 4) that the hardness of B<sub>2</sub>N<sub>3</sub> (52 GPa for both tetragonal and hexagonal polymorphs) is only slightly lower than that of cubic (55 GPa) and wurtzite (54 GPa) BN polymorphs. In contrast, the hardness of B<sub>3</sub>N<sub>3</sub> is significantly lower, especially for the tetragonal polymorph (42 GPa). However, all four new boron nitrides have Vickers hardness exceeding 40 GPa, making them members of the superhard phases family.

The fracture toughness of new boron nitrides decreases from 5.5 MPa·m<sup>1/2</sup> for *h*-B<sub>2</sub>N<sub>3</sub> down to 3.8 MPa·m<sup>1/2</sup> for *tet*-B<sub>3</sub>N<sub>3</sub>, exceeding that of cubic BN ( $K_{Ic} = 2.8 \text{ MPa}\cdot\text{m}^{1/2}$  [39]).

### Energy-volume equations of state

To determine energy trends when considering different crystal structures of a solid, it is necessary to establish the corresponding equations of state (EOS). It is important to note that one cannot rely only on the quantities obtained from lattice optimizations alone, especially when comparing the energies and volumes of different phases. The underlying physics means that the calculated total energy corresponds to the cohesion within the crystal, and the solutions to the Kohn-Sham DFT equation give the energy in terms of infinitely separated electrons and nuclei. The zero of the energy depends on the choice of the atomic potentials (projector augmented waves PAW as here, ultra-soft pseudo-potentials US-PP, etc.); then it becomes arbitrary by its shift, not by scaling. However, the energy derivatives and the EOS remain unchanged. Therefore, it is necessary to obtain the EOS and extract the fit parameters to evaluate the equilibrium values. This was done by a series of calculations of the total energy as a function of volume for the tetragonal and hexagonal phases of new B-N compounds. The resulting  $E(V)$  curves, shown in Fig. 5, were fitted to the third-order Birch equations of state [42]:

$$E(V) = E_0(V_0) + (9/8) \cdot V_0 B_0 [((V_0)/V)^{2/3} - 1]^2 + (9/16) \cdot B_0 \cdot (B' - 4) \cdot V_0 [((V_0)/V)^{2/3} - 1]^3,$$

where  $E_0$ ,  $V_0$ ,  $B_0$ , and  $B'$  are the equilibrium energy; volume; bulk modulus; and its first pressure derivative, respectively. The calculated values are summarized in Table 5. In the case of boron sesquinitride B<sub>2</sub>N<sub>3</sub> (Fig. 5a), the  $E(V)$  curve of *tet*-B<sub>2</sub>N<sub>3</sub> remains at slightly lower energy and higher volume than *h*-B<sub>2</sub>N<sub>3</sub>, but both curves remain close. Quantitatively, this is translated by close equilibrium values (Table 5) due to the close densities of the two phases. Larger differences are observed for the equiatomic phases (Fig. 5b), where the tetragonal B<sub>3</sub>N<sub>3</sub> systematically has lower energy and larger volume than the hexagonal one. An intersection of the  $E(V)$  curves is observed at a volume of 9.74 Å<sup>3</sup> per BN formula unit. The corresponding pressure of

200(30) GPa was estimated by the Murnaghan equation [43] using the  $V_0$ ,  $B_0$  and  $B'$  values from Table 5.

As can be seen from the Fig. 5b, both  $B_3N_3$  polymorphs are metastable with respect to cubic BN over the whole range of experimentally accessible pressures. Nevertheless, the closeness of their cohesive energies allows for the possibility of the formation of both  $B_3N_3$  polymorphs at high pressures and high temperatures as a result of alternative metastable behavior.

## **Dynamic and thermodynamic properties**

### *Phonons band structures*

To verify the dynamic stability of the new B–N phases, an analysis of their phonon properties was performed. The phonon band structures obtained from a high resolution of the tetragonal and hexagonal Brillouin zones in accordance with the method proposed by Togo *et al.* [28] are presented in Fig. 6. The bands (red lines) develop along the main directions of the tetragonal (or hexagonal) Brillouin zone (horizontal  $x$ -axis), separated by vertical lines for enhanced visualization, while the vertical direction ( $y$ -axis) represents the frequencies  $\omega$ , given in terahertz (THz).

The band structures include  $3N$  bands: three acoustic modes starting from zero energy ( $\omega = 0$ ) at the  $\Gamma$  point (the center of the Brillouin zone) and reaching up to a few terahertz, and  $3N-3$  optical modes at higher energies. The low-frequency acoustic modes are associated with the rigid translation modes (two transverse and one longitudinal) of the crystal lattice. The calculated phonon frequencies are all positive, indicating that the four new B–N phases are dynamically stable.

In the case of the tetragonal phases, besides the dispersed bands, the flat bands at  $\sim 39$  THz for  $B_3N_2$  (Fig. 6a) and the higher frequency band at  $\sim 58$  THz for  $B_3N_3$  (Fig. 6b) are observed. The 39-THz band for tetragonal  $B_2N_3$  can be attributed to the B–N distance within the tetrahedron, while the 58-THz band for tetragonal  $B_3N_3$  can be assigned to the B–N distance in the B–N–B fragment along the  $c$ -axis. For hexagonal phases such flat bands are absent while observed bands with frequencies of about 40 THz are due to the larger B–N distances in these phases (see Table 2).

### *Temperature dependence of the heat capacity*

The thermodynamic properties of the new B–N phases were calculated from the phonon frequencies using the statistical thermodynamic approach [44] on a high-precision sampling mesh in the Brillouin zone. The temperature dependencies of the heat capacity at constant volume ( $C_V$ ) for all new boron nitrides are presented in Fig. 7; for  $B_3N_3$  in comparison with the available experimental  $C_p$  data for cubic BN [45]. The heat capacity of tetragonal  $B_2N_3$  is slightly higher than that of the hexagonal phase (Fig. 7a), while the opposite is observed for  $B_3N_3$  (Fig.



7b). The heat capacities of both  $B_3N_3$  polymorphs are slightly higher than that of cubic BN, which is consistent with their more open structures compared to the dense cubic structure. The observed excellent agreement between the calculated and experimental data for cBN supports the validity of the method used to estimate the thermodynamic properties of new boron nitrides.

### Electronic band structures

The electronic band structures of the new boron nitrides were calculated using the all-electrons DFT-based augmented spherical wave method (ASW) method [29] using the crystal structure data from Table 1. The results are shown in Fig. 8. The bands (blue lines) develop along the main directions of the respective tetragonal and hexagonal Brillouin zones. The zero energy along the vertical axis is considered with respect to the Fermi level  $E_F$ . For both  $B_2N_3$  polymorphs (Figs. 8a and 8b), bands cross the Fermi level with a tendency toward a weakly metallic behavior. Obviously, a semiconducting behavior is observed for *tet*- $B_3N_3$ , where a small gap is developed (Fig. 8c); hence, the energy reference is now at  $E_V$ , i.e., at the top of the valence band. Finally, *h*- $B_3N_3$  is clearly metallic with several bands crossing  $E_F$  (Fig. 8d). The different behavior observed between the two equiatomic phases can be attributed to the fact that *tet*- $B_3N_3$  has considerably lower energy than *h*- $B_3N_3$ , as shown in Table 2. As a result, its electronic structure is closer to that of cubic BN. Thus, the new B–N phases exhibit different electronic properties.

### Conclusions

The present work represents a challenging prediction of new tetragonal and hexagonal boron nitrides,  $B_2N_3$  and  $B_3N_3$ , from crystal chemistry and first principles using original pentacarbon templates. The crystal chemistry investigations were supported by computations of the ground structures and energy-dependent quantities within the well-established framework of the quantum density functional theory (DFT). All new phases were found to be cohesive. The mechanical stability of the new phases, which follows from the calculated values of the elastic constants, is coupled with their extreme hardness, varying from 45 GPa for *tet*- $B_3N_3$  to 52 GPa for both  $B_2N_3$  polymorphs. Dynamically, all new phases were found to be stable from positive phonon frequencies, and observed high-frequency modes were assigned to the short B–N distances in their crystal structures. Conductive electronic behavior is observed, which varies from small bandgap semiconducting *h*- $B_2N_3$ , to weakly metallic tetragonal  $B_2N_3$  and  $B_3N_3$ , and finally to metallic *h*- $B_3N_3$ . The results obtained are expected to inspire experimental attempts to synthesize new B–N phases at high pressures and high temperatures.

**Author Contributions:** Conceptualization, S.F.M.; methodology, S.F.M. and V.L.S.; investigation, S.F.M. and V.L.S.; formal analysis, S.F.M. and V.L.S.; data curation, S.F.M. and V.L.S.; visualization, S.F.M. and V.L.S.; validation, S.F.M. and V.L.S.; resources, S.F.M.; writing – original draft preparation, S.F.M.; writing – review and editing, V.L.S. Both authors have read and agreed to the published version of the manuscript.

**Funding:** This research received no external funding.

**Data Availability Statement:** The data presented in this study are available on reasonable request.

**Conflicts of Interest:** The authors declare no conflict of interest.

## References

1. Öhrström, L.; O’Keeffe, M. Network topology approach to new allotropes of the group 14 elements. *Z. Kristallogr.* **2013**, *228*, 343-346.
2. Matar, S.F.; Eyert, V.; Solozhenko, V.L. Novel ultrahard extended hexagonal C<sub>10</sub>, C<sub>14</sub> and C<sub>18</sub> allotropes with mixed sp<sup>2</sup>/sp<sup>3</sup> hybridizations: Crystal chemistry and ab initio investigations. *C* **2023**, *9*, 11.
3. Solozhenko, V.L.; Matar, S.F. Prediction of novel ultrahard phases in the B–C–N system from first principles: Progress and problems. *Materials* **2023**, *16*, 886.
4. Glass, C.W.; Oganov, A.R.; Hansen, N. USPEX – Evolutionary crystal structure prediction. *Comput. Phys. Commun.* **2006**, *175*, 713-720.
5. Zhang, S.; He, J.; Zhao, Z.; Yu, D.; Tian, Y. Discovery of superhard materials via CALYPSO methodology. *Chin. Phys. B* **2019**, *28*, 106104.
6. Hohenberg, P.; Kohn, W. Inhomogeneous electron gas. *Phys. Rev. B* **1964**, *136*, 864-871.
7. Kohn, W.; Sham, L.J. Self-consistent equations including exchange and correlation effects. *Phys. Rev. A* **1965**, *140*, 1133-1138.
8. Lin, S.; Xu, M.; Hao, J.; Wang, X.; Wu, M.; Shi, J.; Cui, W.; Liu, D.; Lei, W.; Li, Y. Prediction of superhard B<sub>2</sub>N<sub>3</sub> with two-dimensional metallicity. *J. Mater. Chem. C* **2019**, *7*, 4527.
9. Juárez, A.R.; Ortíz-Chi, F.; R. Pino-Ríos, R.; Cárdenas-Jirón, G.; Villanueva, M.S.; Anota, E.C. The boron nitride B<sub>116</sub>N<sub>124</sub> fullerene: Stability and electronic properties from DFT simulations. *Chem. Phys. Lett.* **2020**, *741*, 137097.
10. Kurakevych, O.O.; Solozhenko, V.L. Rhombohedral boron subnitride, B<sub>13</sub>N<sub>2</sub>, by X-ray powder diffraction. *Acta Crystallogr. C* **2007**, *63*, i80-i82.
11. Solozhenko, V.L.; Bushlya, V. Mechanical properties of superhard boron subnitride B<sub>13</sub>N<sub>2</sub>. *J. Superhard Mater.* **2017**, *39*, 422-426.
12. Kresse, G.; Furthmüller, J. Efficient iterative schemes for ab initio total-energy calculations using a plane-wave basis set. *Phys. Rev. B* **1996**, *54*, 11169.
13. Kresse, G.; Joubert, J. From ultrasoft pseudopotentials to the projector augmented wave. *Phys. Rev. B* **1999**, *59*, 1758-1775.
14. Blöchl, P.E. Projector augmented wave method. *Phys. Rev. B* **1994**, *50*, 17953-17979.
15. Perdew, J.; Burke, K.; Ernzerhof, M. The Generalized Gradient Approximation made simple. *Phys. Rev. Lett.* **1996**, *77*, 3865-3868.
16. Ceperley, D.M.; Alder, B.J. Ground state of the electron gas by a stochastic method. *Phys. Rev. Lett.* **1980**, *45*, 566-569.

17. Press, W.H.; Flannery, B.P.; Teukolsky, S.A.; Vetterling, W.T. Numerical Recipes, 2<sup>nd</sup> ed.; Cambridge University Press: New York, USA, 1986.
18. Blöchl, P.; Jepsen, O.; Anderson, O. Improved tetrahedron method for Brillouin-zone integrations. *Phys. Rev. B* **1994**, *49*, 16223-16233.
19. Methfessel, M.; Paxton, A.T. High-precision sampling for Brillouin-zone integration in metals. *Phys. Rev. B* **1989**, *40*, 3616–3621.
20. Monkhorst, H.J.; Pack, J.D. Special k-points for Brillouin Zone integration. *Phys. Rev. B* **1976**, *13*, 5188-5192.
21. Gaillac, R.; Pullumbi, P.; Coudert, F.X. ELATE: an open-source online application for analysis and visualization of elastic tensors. *J. Phys.: Condens. Matter* **2016**, *28*, 275201.
22. Voigt, W. Über die Beziehung zwischen den beiden Elasticitätsconstanten isotroper Körper. *Annal. Phys.* **1889**, *274*, 573-587.
23. Mazhnik, E.; Oganov, A.R. A model of hardness and fracture toughness of solids. *J. Appl. Phys.* **2019**, *126*, 125109.
24. Chen, X.Q.; Niu, H.; Li, D.; Li, Y. Modeling hardness of polycrystalline materials and bulk metallic glasses. *Intermetallics* **2011**, *19*, 1275-1281.
25. Mukhanov, V.A.; Kurakevych, O.O.; Solozhenko, V.L. The interrelation between hardness and compressibility of substances and their structure and thermodynamic properties. *J. Superhard Mater.* **2008**, *30*, 368-378.
26. Mukhanov, V.A.; Kurakevych, O.O.; Solozhenko, V.L. Hardness of materials at high temperature and high pressure. *Phil. Mag.* **2009**, *89*, 2117-2127.
27. Lyakhov, A.O.; Oganov, A.R. Evolutionary search for superhard materials: Methodology and applications to forms of carbon and TiO<sub>2</sub>. *Phys. Rev. B* **2011**, *84*, 092103.
28. Togo, A.; Tanaka, I. First principles phonon calculations in materials science, *Scr. Mater.* **2015**, *108*, 1-5.
29. Eyert, V. Basic notions and applications of the augmented spherical wave method. *Int. J. Quantum Chem.* **2000**, *77*, 1007-1031
30. Momma, K.; Izumi, F. VESTA3 for three-dimensional visualization of crystal, volumetric and morphology data. *J. Appl. Crystallogr.* **2011**, *44*, 1272-1276.
31. Matar, S.F.; Solozhenko, V.L. The simplest dense carbon allotrope: Ultra-hard body centered tetragonal C<sub>4</sub>. *J. Solid State Chem.* **2022**, *314*, 123424.
32. Shevchenko, A.P.; Shabalin, A.A.; Karpukhin, I.Yu.; Blatov, V.A. Topological representations of crystal structures: generation, analysis and implementation in the TopCryst system. *Sci Technol Adv Mat.* **2022**, *2*, 250-265.

33. Wei, Q.; Zhang, Q.; Yan, H.; Zhang, M.; Wei, B. A new tetragonal superhard metallic carbon allotrope. *J. Alloys Compd.* **2018**, *769*, 347-352.
34. Solozhenko, V.L.; Häusermann, D.; Mezouar, M.; Kunz, M. Equation of state of wurtzitic boron nitride to 66 GPa. *App. Phys. Lett.* **1998**, *72*, 1691-1693.
35. Nagakubo, A.; Ogi, H.; Sumiya, H.; Kusakabe, K.; Hirao, M. Elastic constants of cubic and wurtzite boron nitrides. *App. Phys. Lett.* **2013**, *102*, 241909.
36. Zhang, J.S.; Bass, J.D.; Taniguchi, T.; Goncharov, A.F.; Chang, Y.-Y.; Jacobsen, S.D. Elasticity of cubic boron nitride under ambient conditions. *J. Appl. Phys.* **2011**, *109*, 063521.
37. Mukhanov, V.A.; Kurakevych, O.O.; Solozhenko, V.L. Thermodynamic model of hardness: Particular case of boron-rich solids. *J. Superhard Mater.* **2010**, *32*, 167-176.
38. Solozhenko, V.L.; Matar, S.F. High-pressure phases of boron pnictides BX (X = As, Sb, Bi) with quartz topology from first principles. *Crystals* **2024**, *14*, 221.
39. Brookes, C.A. The mechanical properties of cubic boron nitride. in *Proc. Int. Conf. Sci. Hard Mater.* **1986**, 207-220.
40. Taniguchi, T.; Akaishi, M.; Yamaoka, S.; Mechanical properties of polycrystalline translucent cubic boron nitride as characterized by the Vickers indentation method. *J. Am. Ceram. Soc.*, **1996**, *79*, 547-549.
41. Dub, S.; Lytvyn, P.; Strelchuk, V.; Nikolenko, A.; Stubrov, Y.; Petrussha, I.; Taniguchi, T.; Ivakhnenko, S. Vickers hardness of diamond and cBN single crystals: AFM approach. *Crystals*, **2017**, *7*, 369.
42. Birch, F. Finite strain isotherm and velocities for single-crystal and polycrystalline NaCl at high pressures and 300 K. *J. Geophys. Res.* **1978**, *83*, 1257-1268.
43. Murnaghan F.D. The compressibility of media under extreme pressures. *Proc. Nation. Acad. Sci. USA* **1944**, *30*, 244-247.
44. Dove, M.T. Introduction to lattice dynamics. Cambridge University Press: New York, USA, 1993.
45. Solozhenko, V.L.; Gavrichev, K.S. Thermodynamic properties of boron nitride. in: "*Wide Band Gap Electronic Materials*". (eds. M.A. Prelas *et al.*), Kluwer Academic Publishers: Dordrecht, Netherlands, 1995, pp. 377-392.

Table 1 Crystal structure transformations of tetragonal carbon (from C<sub>4</sub> to C<sub>5</sub>) and from 2D-C<sub>4</sub> to 3D-C<sub>5</sub> (hexagonal setups), see text for details.

| Space group<br>Topology    | <i>tet</i> -C <sub>4</sub><br><i>I</i> -4 <i>m</i> 2 (No. 119)<br><b>dia</b> | <i>tet</i> -C <sub>5</sub><br><i>P</i> -4 <i>m</i> 2 (No. 115)<br><b>3,4<sup>2</sup>T1-CA</b> | 2D C <sub>4</sub><br><i>P</i> 6 <i>mm</i> (No. 184)<br><b>hcb</b> | 3D C <sub>5</sub><br><i>P</i> -6 <i>m</i> 2 (No. 187)<br><b>lon</b>                    |
|----------------------------|--|---|---|--|
| <i>a</i> , Å               | 2.527  | 2.48  | 2.461   | 2.487  |
| <i>c</i> , Å               | 3.574  | 4.99  | 6.698   | 5.581  |
| Atomic positions           | C1a (½, ½, ½) →<br>C1b (0, 0, 0) →<br>C2a (½, 0, ¼) ] →<br>C2b (0, ½, ¾) ]   | C1 (1c) (½, ½, ½)<br>C2 (2e) (0, 0, ±z)<br>z = 0.313<br>C3 (2g) (0, ½, ±z')<br>z' = 0.854     | C(4b) (⅓, ⅔, 0)   | C1 (2h) (⅓, ⅔, z)<br>z = 0.861<br>C2 (2i) (⅔, ⅓, z')<br>z' = 0.762<br>C'(2f) (⅔, ⅓, ½) |
| E <sub>total</sub> , eV    | -36.38   | -43.26  | -36.87  | -42.51   |
| E <sub>coh/atom</sub> , eV | -2.49  | -2.05   | -2.67   | -1.9   |

N.B. E(C) = -6.6 eV. E<sub>coh/atom</sub> (diamond) = -2.49 eV.

Table 2 Crystal structure parameters of new B–N phases.

| Space group<br>Topology            | <i>tet</i> -B <sub>2</sub> N <sub>3</sub><br><i>P</i> -4 <i>m</i> 2 (No. 115)<br><b>3,4<sup>2</sup>T1-CA</b> | <i>tet</i> -B <sub>3</sub> N <sub>3</sub><br><i>P</i> -4 <i>m</i> 2 (No. 115)<br><b>3,4<sup>2</sup>T1-CA</b> | <i>h</i> -B <sub>2</sub> N <sub>3</sub><br><i>P</i> -6 <i>m</i> 2 (No. 187)<br><b>lon</b> | <i>h</i> -B <sub>3</sub> N <sub>3</sub><br><i>P</i> -6 <i>m</i> 2 (No. 187)<br><b>tfi</b> |
|------------------------------------|--|--|---|---|
| <i>a</i> , Å                       | 2.523  | 2.636  | 2.564   | 2.541   |
| <i>c</i> , Å                       | 4.944  | 6.110  | 5.504   | 7.020   |
| V <sub>cell</sub> , Å <sup>3</sup> | 31.47  | 42.45  | 31.33   | 39.25   |
| Density, g/cm <sup>3</sup>         | 3.358  | 2.913  | 3.374   | 3.150   |
| Shortest B–N bond, Å               | 1.35   | 1.32   | 1.41  | 1.44  |
| Atomic positions                   | B1(2g) (0, ½, 0.310)<br>N1 (2e) (0, 0, 0.863)<br>N2 (1c) (½, ½, ½)   | B1(2g) (0, ½, 0.353)<br>B2(1a) (0, 0, 0)<br>N1(2e) (0, 0, 0.783)<br>N2(1c) (½, ½, ½)                         | B (2i) (⅔, ⅓, 0.757)<br>N1(2h) (⅓, ⅔, 0.865)<br>N2(1f) (⅔, ⅓, ½)                          | B1 (2i) (⅔, ⅓, 0.704)<br>B2 (1c) (⅓, ⅔, 0)<br>N1(2h) (⅓, ⅔, 0.209)<br>N2(1f) (⅔, ⅓, ½)    |
| E <sub>total</sub> , eV            | -40.76   | -49.43   | -39.78  | -46.42  |

Table 3 Elastic constants ( $C_{ij}$ ) of the new boron nitrides in comparison with those of the original carbon allotropes (all values are in GPa).

|   | $C_{11}$ | $C_{12}$ | $C_{13}$ | $C_{33}$ | $C_{44}$ | $C_{66}$ |
|---|----------|----------|----------|----------|----------|----------|
| <i>tet</i> -C <sub>5</sub>                | 943      | 9        | 136      | 1194     | 198      | 337      |
| <i>tet</i> -B <sub>2</sub> N <sub>3</sub> | 712      | 57       | 164      | 987      | 82       | 307      |
| <i>tet</i> -B <sub>3</sub> N <sub>3</sub> | 614      | 23       | 126      | 928      | 119      | 161      |
| <i>h</i> -C <sub>5</sub>                  | 920      | 95       | 46       | 1453     | 412      | 333      |
| <i>h</i> -B <sub>2</sub> N <sub>3</sub>   | 680      | 137      | 20       | 1416     | 272      | 199      |
| <i>h</i> -B <sub>3</sub> N <sub>3</sub>   | 453      | 124      | 139      | 1190     | 165      | 154      |



Table 4 Mechanical properties of new boron nitrides: Vickers hardness ( $H_V$ ), bulk modulus ( $B$ ), shear modulus ( $G$ ), Young's modulus ( $E$ ), Poisson's ratio ( $\nu$ ) and fracture toughness ( $K_{Ic}$ ). The subscript  $v$  for elastic moduli indicates the use of the Voigt averaging scheme. The # denotes the space group number. The corresponding values for wurtzite and cubic boron nitrides are given for comparison.

|  | $H_V$ |              |               |         | $B$                 |       | $G_V$               | $E_V$             | $\nu_V$             | $K_{Ic}^\ddagger$   |
|--|-------|--------------|---------------|---------|---------------------|-------|---------------------|-------------------|---------------------|---------------------|
|  | $T^*$ | $LO^\dagger$ | $MO^\ddagger$ | $CN^\S$ | $B_0^*$             | $B_V$ |                     |                   |                     |                     |
|  | GPa   |              |               |         |                     |       |                     |                   |                     |                     |
| <i>tet</i> -B <sub>2</sub> N <sub>3</sub> #115 | 52    | 51           | 23            | 26      | 357                 | 353   | 229                 | 566               | 0.233               | 4.5                 |
| <i>h</i> -B <sub>2</sub> N <sub>3</sub> #187   | 52    | 49           | 49            | 51      | 359                 | 348   | 322                 | 738               | 0.146               | 5.5                 |
| <i>tet</i> -B <sub>3</sub> N <sub>3</sub> #115 | 45    | 42           | 21            | 26      | 314                 | 301   | 205                 | 502               | 0.222               | 3.8                 |
| <i>h</i> -B <sub>3</sub> N <sub>3</sub> #187   | 49    | 46           | 22            | 25      | 340                 | 322   | 210                 | 517               | 0.233               | 3.9                 |
| wBN #186                                       | 54    | 50           | 70            | 64      | 375 <sup>[34]</sup> |       | 384 <sup>[35]</sup> | 858 <sup>**</sup> | 0.118 <sup>**</sup> | –                   |
| cBN #216                                       | 55    | 50           | 74            | 69      | 381 <sup>[36]</sup> |       | 399 <sup>[36]</sup> | 890 <sup>**</sup> | 0.107 <sup>**</sup> | 2.8 <sup>[39]</sup> |

\* Thermodynamic model [26]

† Lyakhov-Oganov model [27]

‡ Mazhnik-Oganov model [23]

§ Chen-Niu model [24]

\*\* calculated using isotropic approximation

Table 5. Calculated properties of new boron nitrides: bulk modulus ( $B_0$ ) and its first pressure derivative ( $B_0'$ ); total energy ( $E_0$ ) and equilibrium volume ( $V_0$ ) per formula unit.

|                              | $B_2N_3$          |                  | $B_3N_3$          |                  |
|------------------------------|-------------------|------------------|-------------------|------------------|
|                              | <i>tetragonal</i> | <i>hexagonal</i> | <i>tetragonal</i> | <i>hexagonal</i> |
| $B_0$ (GPa)                  | 344               | 336              | 300               | 317              |
| $B_0'$                       | 3.76              | 3.75             | 3.67              | 3.71             |
| $E_0$ /FU (eV)               | -40.7             | -39.1            | -49.4             | -46.4            |
| $V_0$ /FU ( $\text{\AA}^3$ ) | 31.5              | 42.5             | 31.3              | 39.3             |

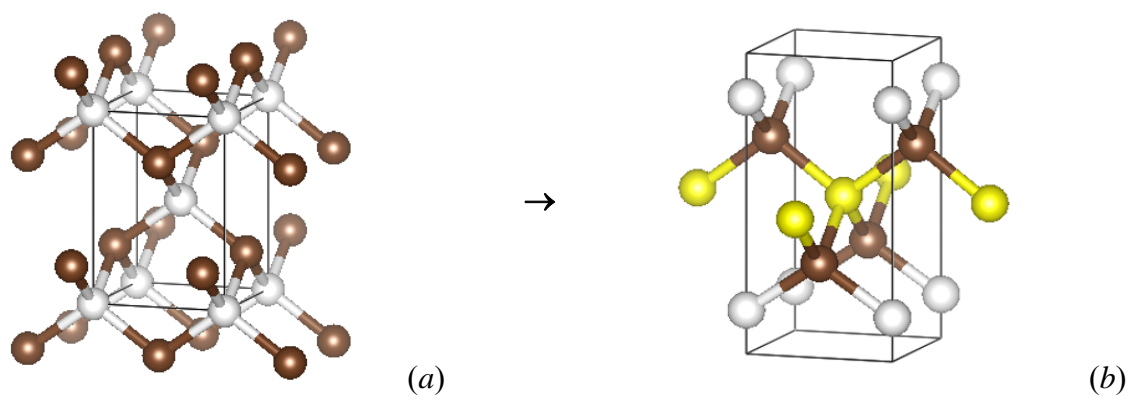


Figure 1 Schematic transformation of *tet-C*<sub>4</sub> (a) to *tet-C*<sub>5</sub> (b) (see Table 1 & text for details). The additional yellow spheres result from the decrease in symmetry.

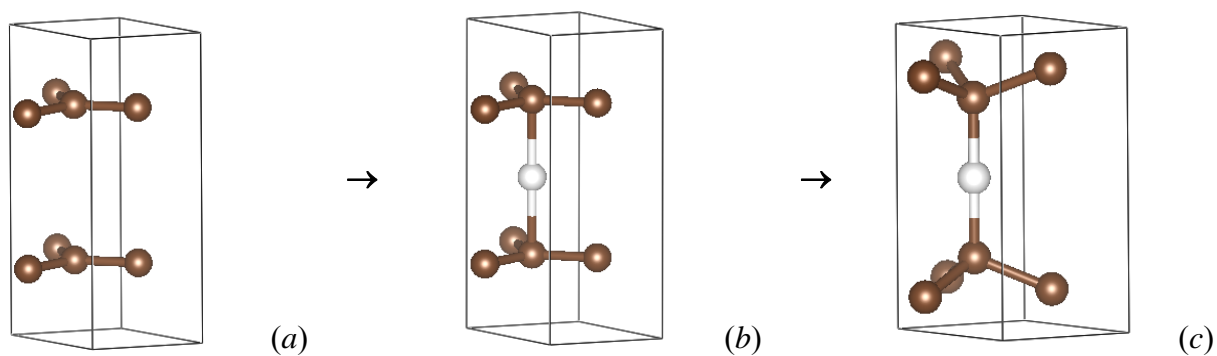


Figure 2 Transformation (and stoichiometry change) from layered *h-C*<sub>4</sub> (a) to *C*<sub>5</sub> (b) by inserting a carbon atom at  $z = \frac{1}{2}$  (white sphere), and the fully geometry-optimized 3D *h-C*<sub>5</sub> (c) (see Table 1 & text).

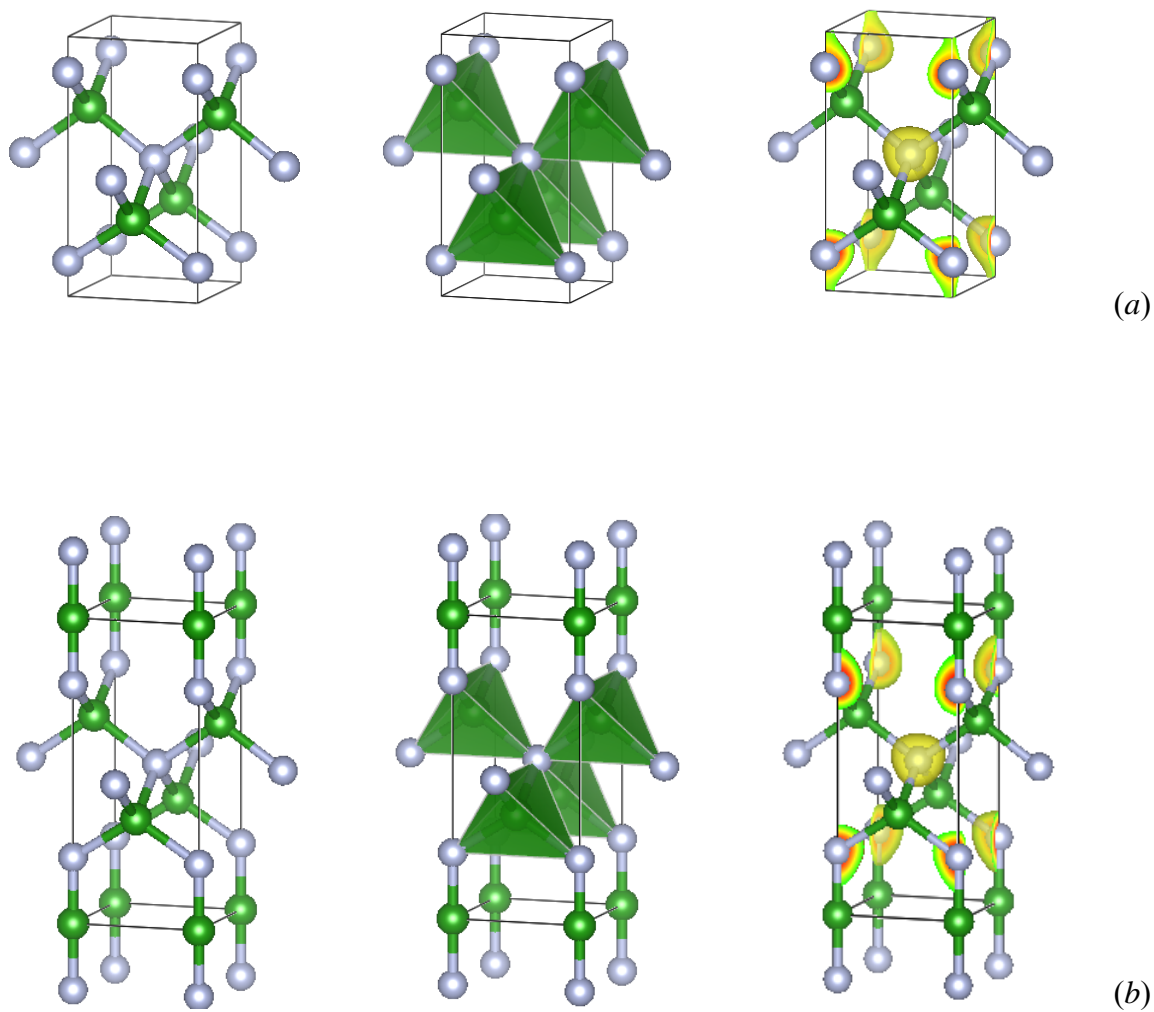


Figure 3. Ball-and-stick (left), polyhedral (middle), and charge projection (right) representations of the crystal structures of new tetragonal  $B_2N_3$  (a) and  $B_3N_3$  (b). Green and gray spheres represent boron and nitrogen atoms, respectively.

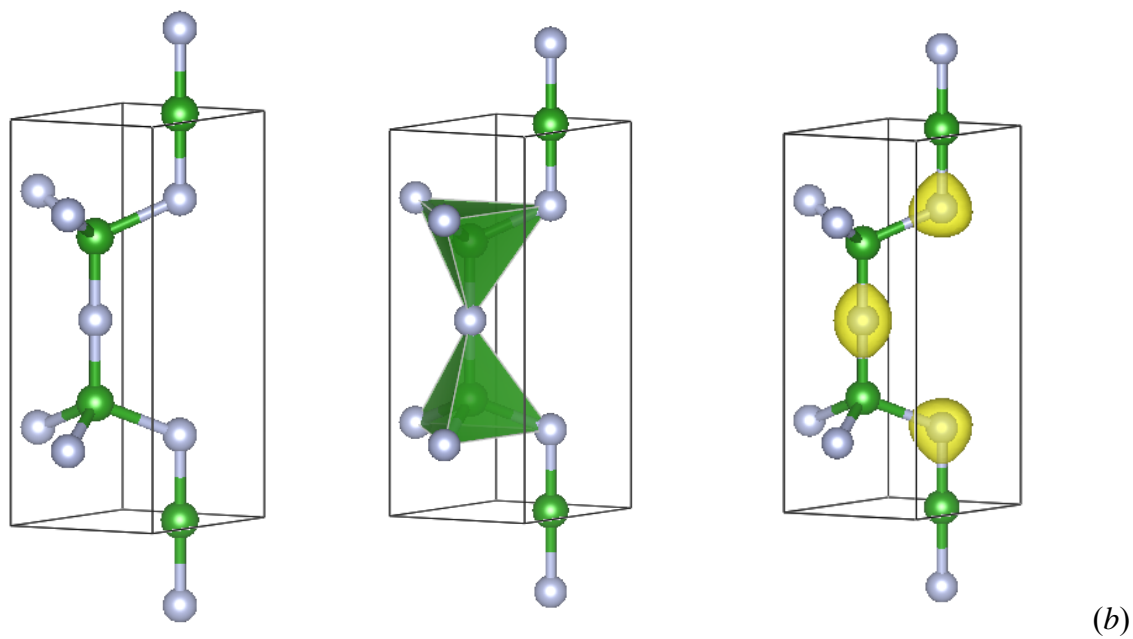
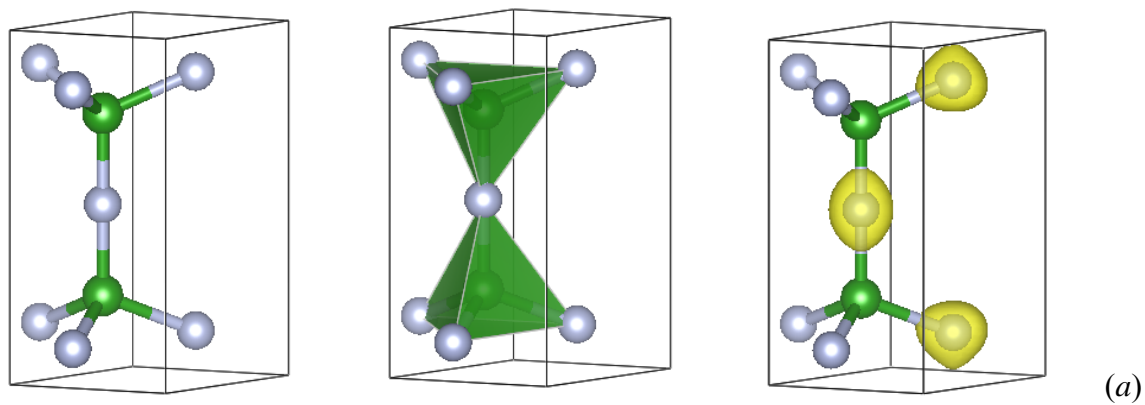
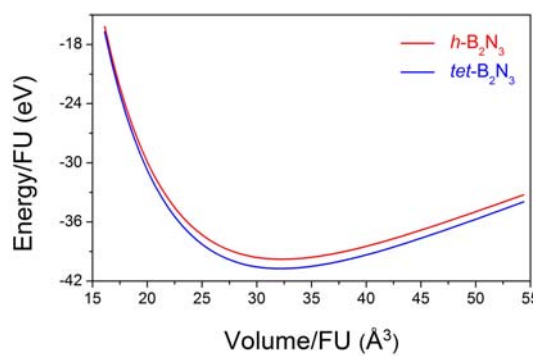
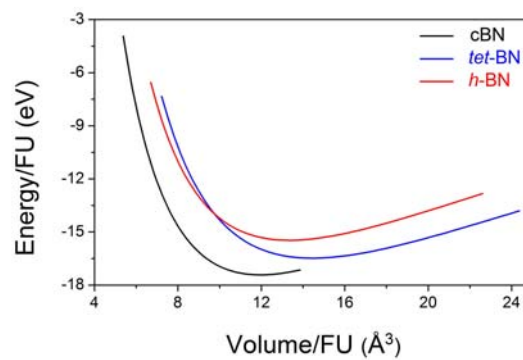


Figure 4. Ball-and-stick (left), polyhedral (middle), and charge projection (right) representations of the crystal structures of new hexagonal  $B_2N_3$  (a) and  $B_3N_3$  (b). Green and gray spheres represent boron and nitrogen atoms, respectively.



(a)



(b)

Figure 5. Calculated total energy as a function of volume for new boron nitrides:  $\text{B}_2\text{N}_3$  (a) and  $\text{B}_3\text{N}_3$  (b). In the case of  $\text{B}_3\text{N}_3$ , all values are given per BN formula unit for comparison with cBN.

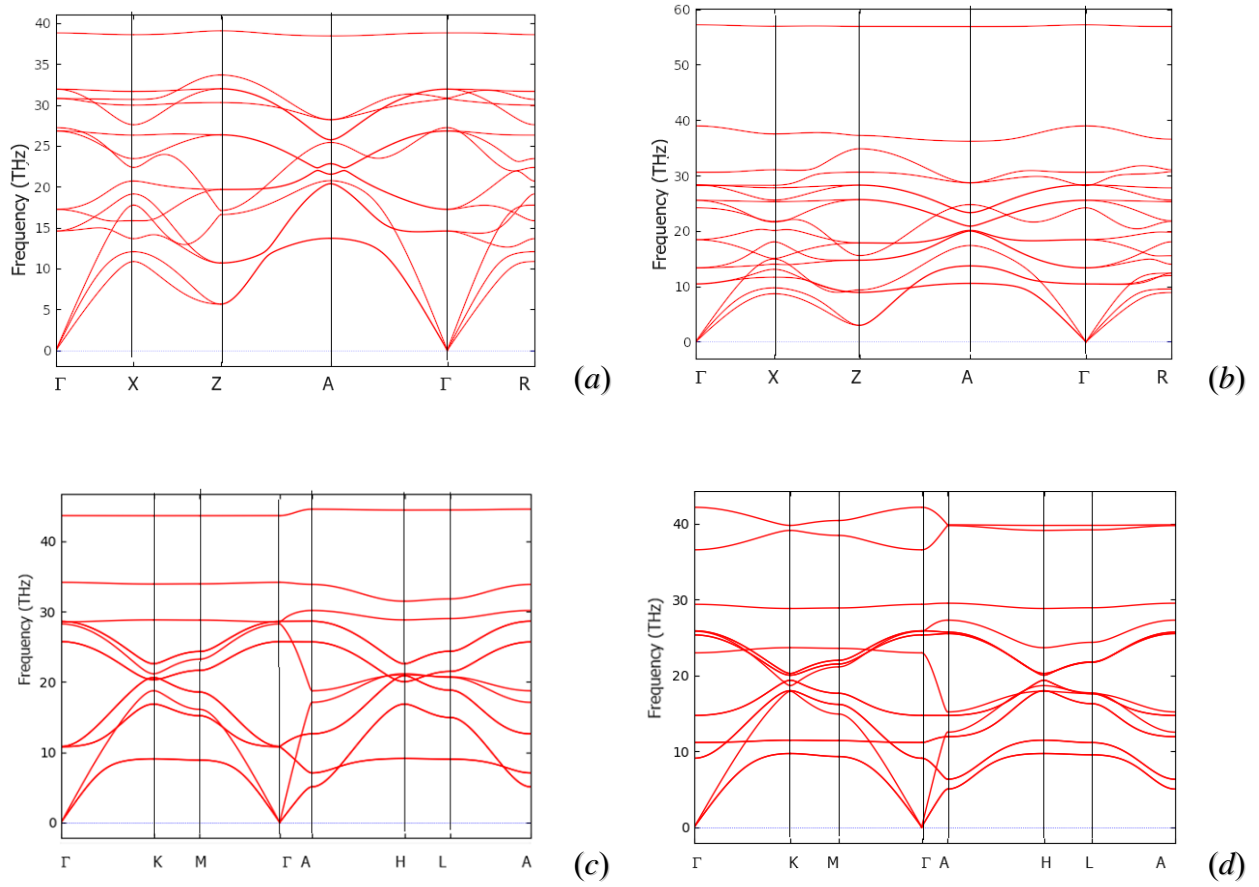
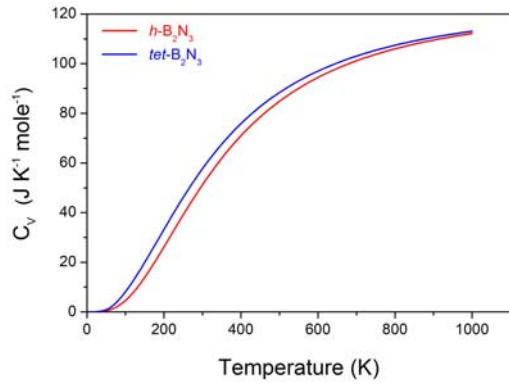
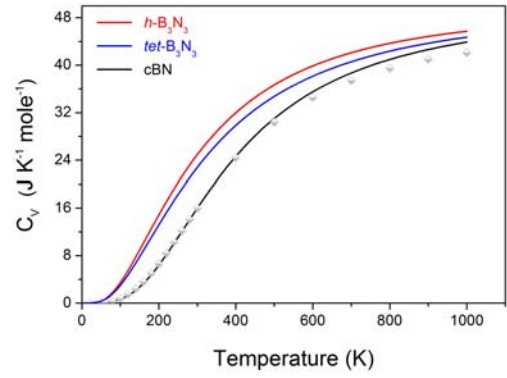


Figure 6 Phonon band structures of new boron nitrides along the major directions of the simple tetragonal (*a,b*) and hexagonal (*c,d*) Brillouin zones: *tet*- $\text{B}_2\text{N}_3$  (*a*); *tet*- $\text{B}_3\text{N}_3$  (*b*); *h*- $\text{B}_2\text{N}_3$  (*c*); *h*- $\text{B}_3\text{N}_3$  (*d*).



(a)



(b)

Figure 7 Heat capacity at constant volume ( $C_V$ ) of new boron nitrides:  $B_2N_3$  (a) and  $B_3N_3$  (b). In the case of  $B_3N_3$ ,  $C_V$  values are given per BN formula unit for comparison with cBN. Experimental heat capacity data for cBN [45] are shown as gray symbols.



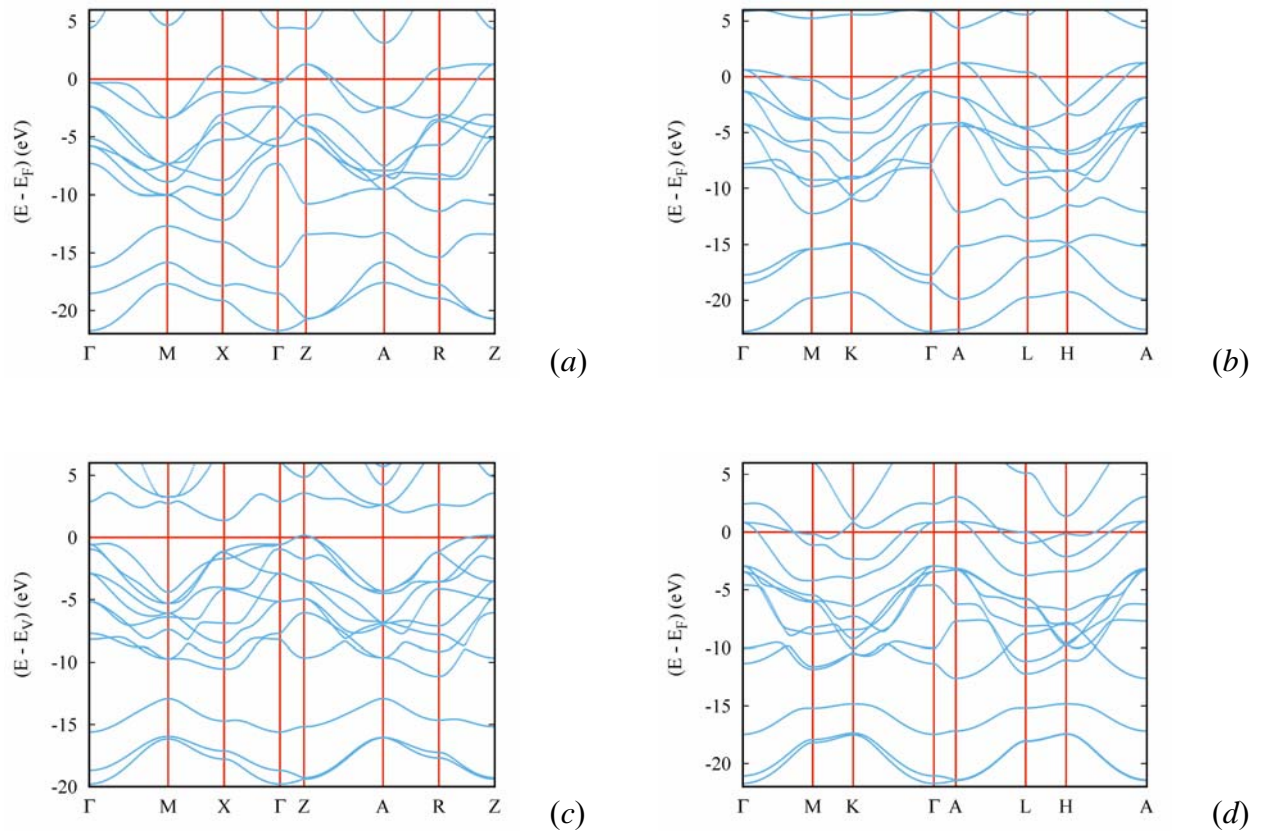


Figure 8 Electronic band structures of new boron nitrides: *tet*-B<sub>2</sub>N<sub>3</sub> (a); *h*-B<sub>2</sub>N<sub>3</sub> (b); *tet*-B<sub>3</sub>N<sub>3</sub> (c); *h*-B<sub>3</sub>N<sub>3</sub> (d).